Chapter 4 : Microstructural evolution and phase stability in semi-Heusler NiMnSb and vanadium added equi-atomic NiMnSbV alloy

4.1 Introduction

Cu_2MnAl Heusler phase, as named after its discoverer Freudrich Heusler, is known for its ferromagnetism even though none of its constituents are magnetic in nature [15]. Since the discovery of the first Heusler phase Cu_2MnAl, several such alloys have been discovered [15], which can be classified on the basis of alloy composition and crystal structure. Structurally these alloys are classified as Heusler, semi-Heusler, quaternary-Heusler and inverse-Heusler. A plethora of functional properties could be achieved in these alloys based on its alloy composition and structure, which are further modified by the presence of defects [117]. However, the structure is not always easy to be determined at the atomic scale with the atoms and the vacancies located in the lattice [118]. Additionally, most of the Heusler phases appear to be similar in terms of projected potential from different crystallographic directions.

Semi-Heusler NiMnSb alloy has regained traction in the recent past due to its potential application as thermoelectric material and in spintronics [119,120]. A closely related NiMnIn semi-Heusler alloy forms decagonal quasicrystal upon rapid solidification [121], which is unique for these alloys as decagonal quasicrystals are mostly found in aluminum alloys. Semi-Heusler alloys e.g. NiMnSb are not strictly stoichiometric [122], its composition may vary within a narrow composition range and it is stable at room temperature. Additionally, it can accommodate interstitial, substitutional and anti-site defects, which further tailors its thermoelectric properties [119]. Presence of antiphase boundaries in Heusler alloys modifies its exchange interactions, however, its ferromagnetic ordering across the interface remains intact [123]. Semi-Heusler NiMnSb alloys with one spin direction shows overlapping valence band and conduction band. However, with opposite spins, it develops finite difference in the valence band and conduction band making this alloy a half metallic ferromagnet [124]. Semi-Heusler NiMnSb alloy shows high resistivity above Curie temperature (~700 K). It is anomalous with respect to other alloys in this class. The magnetization behavior of NiMnSb is also different from similar alloys in this class as it shows small

and declining value of effective magnetic moments above the Neel temperature [125,126].

Binary Ni-Mn phase diagram is complicated with the presence of a good number of intermetallic phases [127]. The lower temperature part of the phase diagram is not unambiguously determined. NiMnSb alloy has been studied through diffusion couples and with diffusion triplets. It is reported that $L2_1$ Heusler phase and the $C1_b$ semi-Heusler phase is stable up to 700 ºC. However, at 900 ºC, only $L2_1$ Heusler phase can be observed without the presence of $C1_b$ semi-Heusler phase [122]. Addition of fourth element may further destabilize the structure. It is important to understand the alloying behavior as it may open up further possibilities for tailoring the properties. With the advent of high entropy alloys (HEAs) [128], it has been reported that substitution of similar elements in the lattice of intermetallic may lead to the formation high entropy intermetallic phases [129].

In the present study, semi-Heusler NiMnSb and NiMnSbV alloy has been synthesized through solidification route (induction melting) in order to study the phase, microstructure evolution and stability of the alloys. It has been attempted to explain the microstructural evolution and phase stability in these alloys in the frame work of thermodynamics and other heuristic approaches those are used to design alloys.

4.2 Experimental techniques

High purity granules of nickel (99.9%, Alfa Aesar), manganese (99.9%, Alfa Aesar), antimony (99.0%, Alfa Aesar), vanadium (99.8%, Alfa Aesar) were taken in stoichiometric proportion in a recrystallized alumina crucible and it was melted in a vacuum induction melting furnace (VIM) under inert Ar atmosphere to obtain equi-atomic NiMnSb and NiMnSbV alloys. The furnace chamber was evacuated and it was purged with Ar gas before the mixture was heated. The melting was carried out at ~1100ºC and the melt was allowed to homogenize for 15 minutes. The melting process was repeated for three times in order to ascertain the compositional homogenization. The melt was allowed to cool down in the recrystallized alumina crucible. The induction melted alloy was sliced by a slow speed diamond saw and both sides of the slice was polished for x-ray diffraction studies. X-ray diffraction (XRD) experiments were

performed using Rigaku Mini Flex 600 with Cu-K_α radiation (~1.543 Å) with 40 kV accelerating voltage and 15 mA tube current. Samples were scanned from 25° to 90°, with a step size of 0.01° and scan rate of 5°/min. Rietveld refinement of the experimental x-ray diffraction patterns were done by FullProf software. The models of different co-ordination environments have been investigated with the help of Vesta software. Heating stage XRD measurements were done at 200ºC, 400ºC, 600ºC and 700ºC with the heating rate of 5ºC/min and holding time of two hours at the respective temperatures using a Rigaku Smart Lab 9kW Powder type x-ray diffractometer. TEM samples were prepared by crushing the NiMnSb and NiMnSbV alloy into the powder form in a mortar and pestle. The powder was suspended in ethanol and it was ultra-sonicated for 15 minutes before it was drop cast onto a carbon coated copper grid. The Microscopy was carried out using a Tecnai G^2T20 LaB_6 TEM operating at 200 kV.

4.3 Results

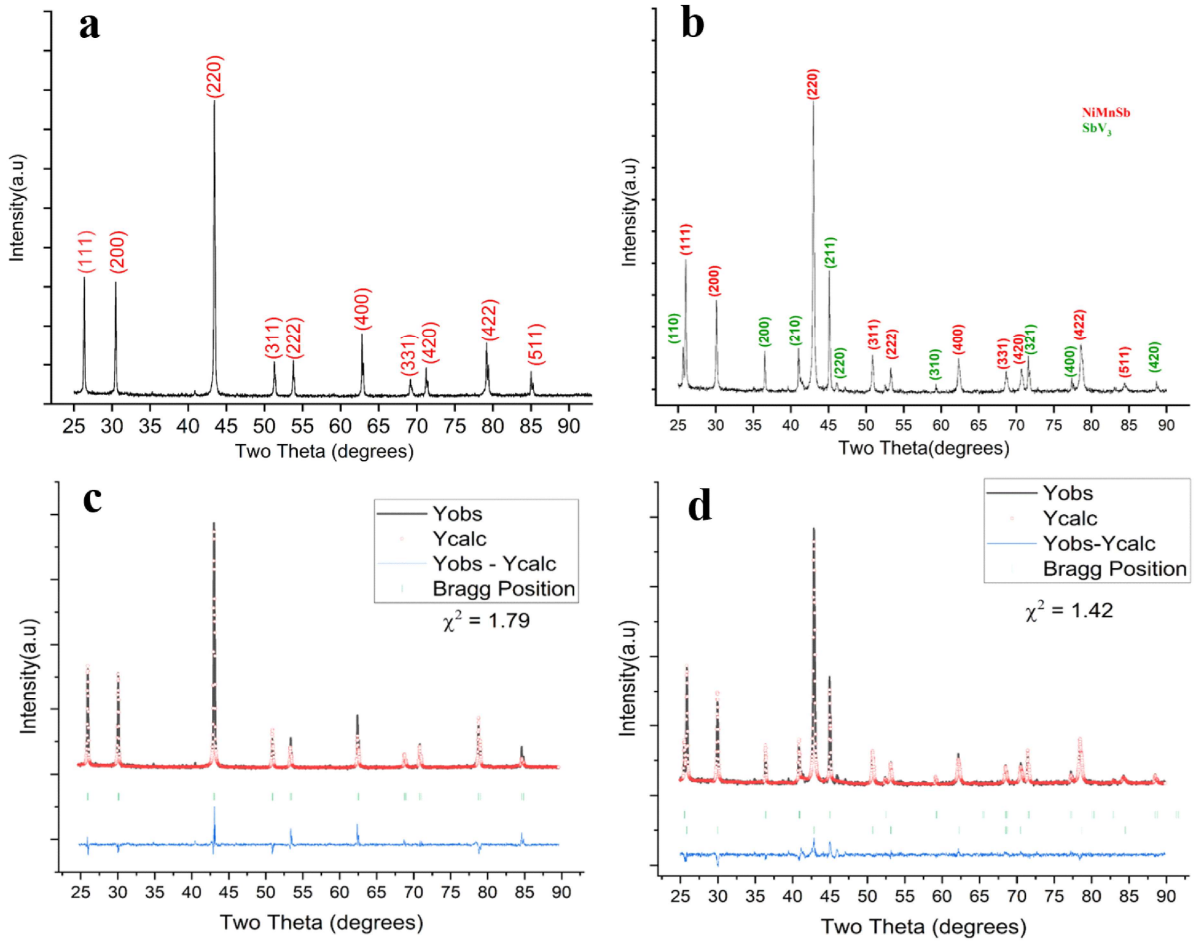

Figure 4.1: XRD pattern of induction melted and as-solidified (a) NiMnSb semi-Heusler alloy, which shows only standard FCC reflections (b) NiMnSbV alloy, which shows additional SbV_3 reflections (marked in green) along with the standard reflections from the semi-Heusler NiMnSb phase. (c) Rietveld refined pattern (χ^2 = 1.79) of (a) which confirms the presence of FCC semi-Heusler NiMnSb phase only (d) Rietveld refined pattern (χ^2 = 1.42) of (b) which confirms the presence of cubic SbV_3 phase along with the cubic semi-Heusler NiMnSb phase.

The XRD pattern of induction melted and as-solidified semi-Heusler NiMnSb is shown in Fig 4.1(a). The XRD pattern indicates that the alloy is completely crystalline after induction melting and cooling in the recrystallized alumina crucible. The diffraction peaks are sharp, which necessarily indicates that the grains are coarse and it is almost strain free. The XRD peaks can be indexed to the FCC structure of NiMnSb (Pearson Symbol: cF12) semi-Heusler phase with space group $F\bar{4}3m$ and with lattice

parameter a= 5.92 Å. The reflections on the higher angle side show minor split and the intensity of the reflections is also small. This could be attributed to the $K\alpha_2$ reflection, otherwise it might be due the cubic to tetragonal polymorphic transformation [130] of the NiMnSb semi-Heusler alloy. However, similar split of the diffraction peaks could not be observed at the lower angle side. Some very low intense peaks can be observed in the pattern which lacks in terms of consistency of Bragg position have not been indexed. In order to substantiate the proposition, Rietveld refinement of the diffraction pattern was done. The Rietveld refined data (Figure 4.1c) matches quite accurately with the cF12 NiMnSb semi-Heusler phase with a=5.92 Å. It can be concluded from this observation that the induction melted and as solidified NiMnSb alloy is cubic single phase and it rules out the possibility of existence of any tetragonal polymorph or any other second phase in the alloy.

The XRD pattern of induction melted and as-solidified NiMnSbV alloy (Figure 4.1b) shows sharp crystalline peaks, which could be indexed to semi-Heusler NiMnSb alloy (SG: $F\bar{4}3m$, Pearson Symbol cF12, a= 5.92 Å) and SbV_3 phase (SG: $Pm\bar{3}n$, Pearson Symbol: cP8, a=4.94 Å). The peaks are quite sharp indicating that the alloy is purely crystalline and the grains are coarse and strain free. Intensities of the diffraction peaks of the two phases may qualitatively indicate that the volume fraction of the semi-Heusler NiMnSb phase is fairly large with respect to the SbV_3 phase. The diffraction peaks of the NiMnSb phase at the higher angle side are little asymmetric. However, the split is not evident. In order to confirm the absence of any other polymorphically related phase, multiphase Rietveld refinement of the XRD pattern was done. The Rietveld refined pattern (Figure 4.1d) confirms the presence of cubic NiMnSb semi-Heusler and cubic SbV_3 phases. However, no other third phase or polymorphically related phase could be confirmed.

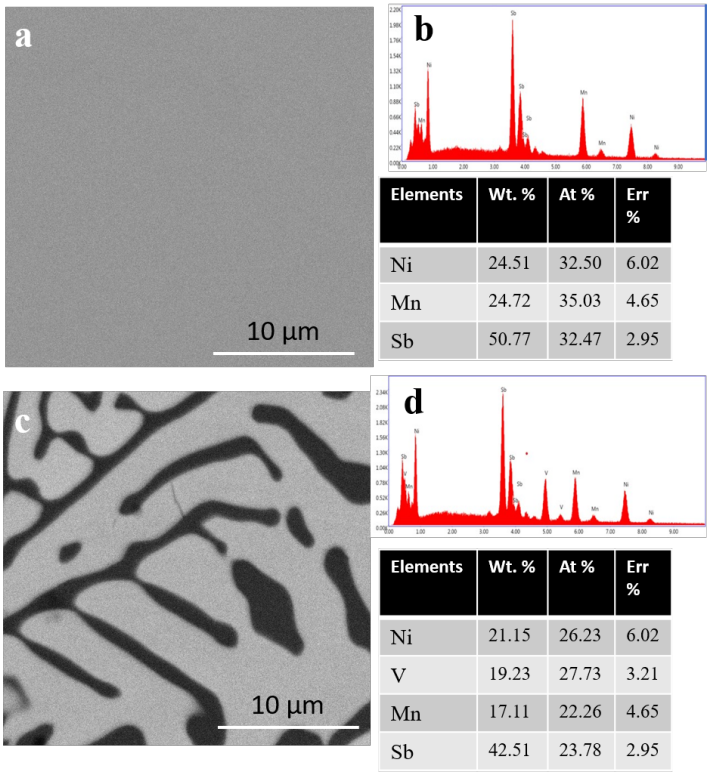

Elements	Wt. %	At %	Err %
Ni	24.51	32.50	6.02
Mn	24.72	35.03	4.65
Sb	50.77	32.47	2.95

Elements	Wt. %	At %	Err %
Ni	21.15	26.23	6.02
V	19.23	27.73	3.21
Mn	17.11	22.26	4.65
Sb	42.51	23.78	2.95

Figure 4.2: (a) SEM micrograph (b) XEDS spectra of induction melted and as-solidified NiMnSb alloy. In the SEM micrograph solidification shrinkage porosities are observed and in the XEDS spectra almost equi-atomic distribution of Ni, Mn and Sb is observed. (c) SEM micrograph (d) XEDS spectra of the SbV_3 phase in the induction melted and as-solidified NiMnSbV alloy. In the SEM micrograph, along with solidification shrinkage porosities, semi-Heusler NiMnSb and cubic SbV_3 phases are observed. Lamellar structures at the interface of two phases are present. The SbV_3 phase is almost stoichiometric as confirmed from the XEDS spectra in (d).

SEM micrograph of the as-solidified NiMnSb alloy (Figure 4.2a) shows usual solidification defects i e. porosities etc., otherwise no trace of second phase is observed in this alloy. The X-ray energy dispersive spectrum (XEDS) (Figure 4.2b) from the same region shows only Ni, Mn and Sb. The Ni, Mn and Sb are present in ~37.7%, 33.1% and 29.2% (at%) respectively. This further reinforces the XRD observation that the alloy is single phase. The composition of the alloy is nearly equi-atomic considering the error that may be present in XEDS measurement. Additionally, it must be emphasized that the melting point of Sb is ~630 ºC, which is considerably lower than Ni and Mn (melting point of Ni and Mn are ~1454ºC and 1246ºC). The boiling point of Sb is ~1635ºC. The

partial vapor pressure of Sb increases steeply with the increase in temperature. Even though, the melting and homogenization was done under Ar back pressure, it might be possible that minor loss of Sb took place during the process, which has resulted in lowering of the atomic percent of Sb in the alloy. This further confirms that semi-Heusler NiMnSb is not perfectly stoichiometric compound. SEM micrograph of the as solidified NiMnSbV alloy (Figure 4.2c) indicates that the alloy consists of two phases. Usual solidification defects e.g. porosities are present in the alloy. The phases are distinguished by grey and white contrast. The XEDS spectra from the grey phase (Figure 4.2d) indicates that in this phase Ni, Mn, Sb and V are present in ~1.9 at%, 4.4 at%, 22.7 at% and 71.1 at% respectively. This confirms that the phase is SbV_3. The presence of this phase was confirmed through XRD also. However, it can be said that the SbV_3 phase is not perfectly stoichiometric, it has accommodated minor quantities of Ni and Mn also. Similarly, the XEDS spectra from the white phase indicates that in this phase Ni, Mn, Sb and V are present in 32.5 at%, 36 at%, 29.5 at% and 2 at% respectively. The composition profile indicates that the white phase is nearly equi-atomic in terms of Ni, Mn and Sb with very minor amount of V. The white phase is semi-Heusler NiMnSb. The same phase was observed in XRD also. The composition also indicates that the phase is not strictly stoichiometric, which was observed in case of a NiMnSb alloy also.

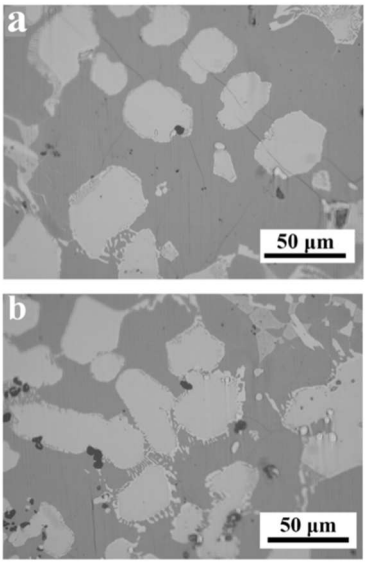

Figure 4.3(a-b): Visible light micrograph of induction melted and as-solidified NiMnSbV alloy in which mildly faceted islands of SbV_3 phase in the matrix of semi-Heusler NiMnSb phase is observed. Lamellar structure is quite often observed at the interface of the two phases.

Visible light micrographs of as solidified NiMnSbV alloy (Figure 4.3(a-b)) shows islands of SbV_3 phase inhomogeneously distributed in the matrix of NiMnSb. The SbV_3 phase is blocky and irregular in shape. The size of the phase varies in the range of ~50-100 µm. In some of the interfaces of SbV_3 and NiMnSb phases, fine lamellar structure (Figure 4.3b) is observed. The width of the lamella is ~1-2 µm. Similar lamellar structure is observed in the SEM micrograph of the same alloy in Figure 4.2(c). The solidification microstructure provides important mechanism about the solidification behavior of the NiMnSbV alloy.

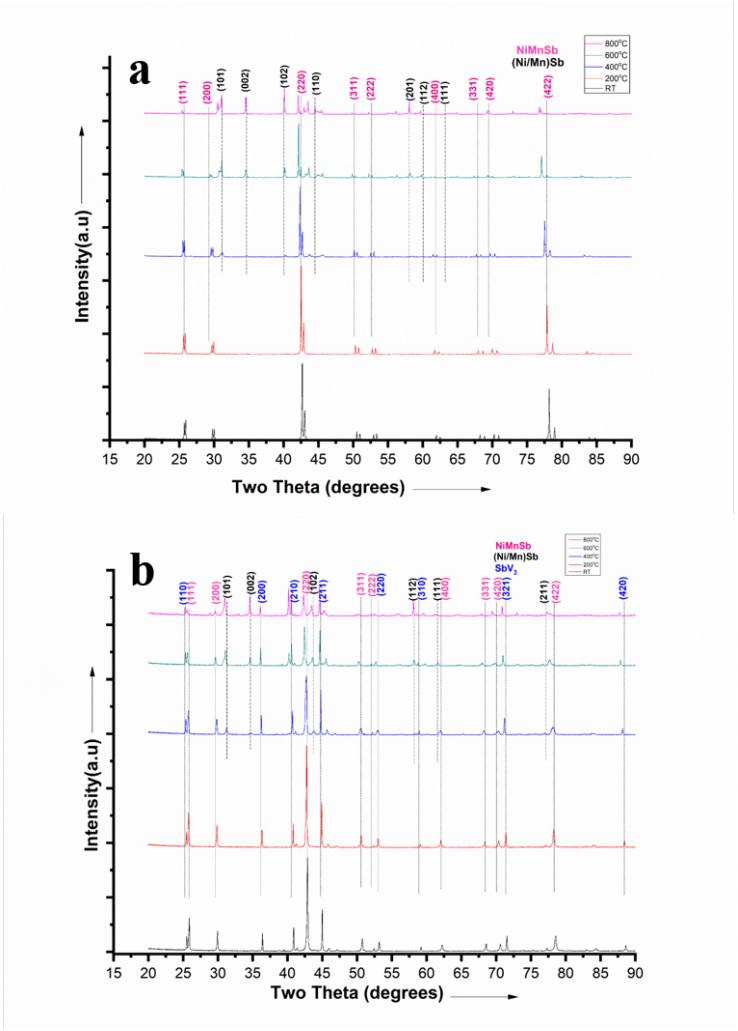

Figure 4.4: Multiple display of in-situ XRD patterns of induction melted and as-solidified (a) NiMnSb, (b) NiMnSbV alloy recorded at room temperature (RT), 200, 400, 600 and 700 °C. In both the alloys, from 400 °C, hexagonal (Ni/Mn)Sb phase evolves at the expense of the cubic semi-Heusler NiMnSb parent phase while the cubic SbV_3 phase appears to be stable in the temperature range of investigation.

In-situ high temperature XRD patterns of the NiMnSb alloy is given in Figure 4.4(a). The NiMnSb alloy was heated to 200, 400, 600 and 700 ºC and it was held at that temperature for two hours before the diffraction pattern was recorded. In Figure 4.4(a), the room temperature XRD pattern of NiMnSb semi-Heusler phase is given for direct reference. When the alloy is heated to 200 ºC, the XRD pattern does not show any detectable change. At 400 ºC, apart from the XRD peaks corresponding to semi-Heusler NiMnSb phase, a number of low intensity peaks could be observed (marked with the dotted line in Figure 4.4(a). At 600 ºC the intensity of the new peaks become prominent and they become even more prominent at 700 ºC. The diffraction intensities of the new phase become prominent at the cost of the initial intensities of the NiMnSb phase. It can be concluded from this observation that the volume fraction of the new phase grows at the cost of the NiMnSb semi-Heusler phase. The new phase could be indexed to hexagonal NiSb phase (SG: $P6_3/mmc$; Pearson Symbol: hP4; a = 3.935 Å and c = 5.136 Å). However, the MnSb phase is isostructural with the NiSb phase (SG: $P6_3/mmc$; Pearson Symbol: hP4; a= 4.149 Å and c= 5.771 Å) with very similar lattice parameter. This observation confirms that the semi-Heusler NiMnSb phase is not stable beyond 400 ºC. Isostructural NiSb/MnSb phase nucleates at the expense of NiMnSb phase and it grows in volume fraction with high temperature heat treatment. The new phase could be considered as the solid solution phase of NiSb and MnSb; and it is better represented as (Ni/Mn)Sb.

The in-situ high temperature XRD patterns of the NiMnSbV alloy are given in Figure 4.4b as multiple display. In conformity with the NiMnSb alloy, this alloy was also heated to 200, 400, 600, 700 ºC, it was held at those temperatures for two hours before the XRD pattern was recorded. The original room temperature XRD pattern of the NiMnSbV alloy is given at the bottom of the multiple display in Figure 4.4(b) for ready reference. Similar to the NiMnSb alloy, the two phase NiMnSbV alloy consisting of semi-Heusler NiMnSb and SbV_3 phases are stable upto 400 ºC. At 400 ºC, minor diffraction peaks are observed (marked by dotted line in Figure 4.4(b), which grow considerably at 600 and 700 ºC at the cost of the initial diffraction intensities of the semi-Heusler NiMnSb phase. The diffraction intensities of the SbV_3 phase remains almost intact. This observation is in line with the observation reported in Figure 4.4a for NiMnSb alloy. As the phase is not stable beyond 400 ºC, (Ni/Mn)Sb phase nucleates at

the expense of parent NiMnSb semi-Heusler phase. However, there is no change in the XRD signature of SbV_3 phase and it is assumed to be stable in the temperature regime of investigation over the length of time for which the isothermal holding was carried out.

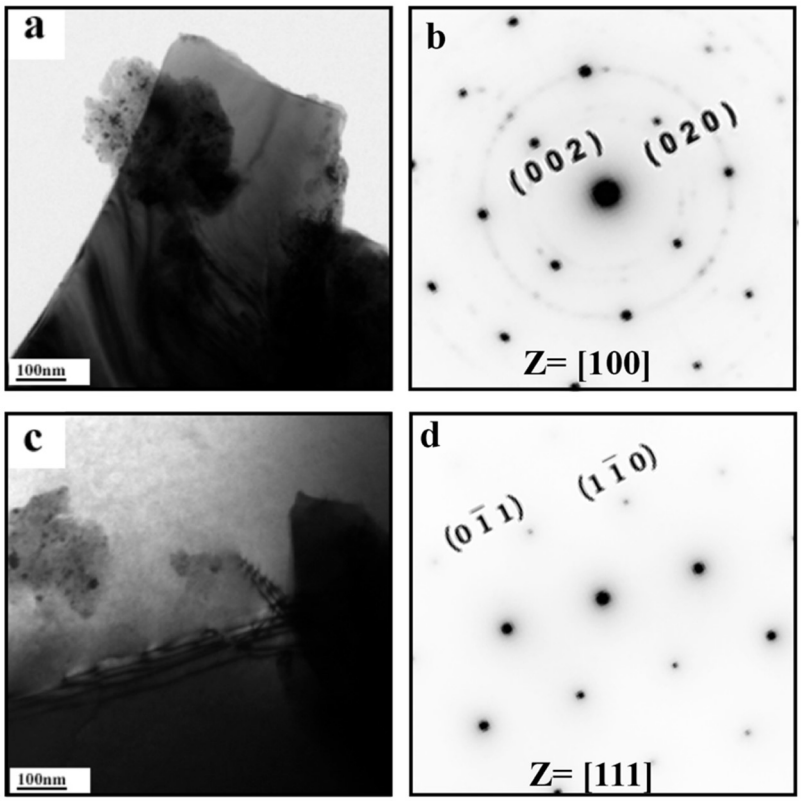

Figure 4.5: (a, c) TEM bright field images (b, d) corresponding rotationally oriented electron diffraction patterns from the induction melted and as-solidified NiMnSb semi-Heusler alloy. In the bright field images of the semi-Heusler phase, bend contours and dislocations are observed. Electron diffraction patterns along Z=[100] in (c) and Z=[111] in (d) confirms the cubic structure of the semi-Heusler phase.

TEM bright field image of as-solidified NiMnSb alloy and its corresponding diffraction pattern are given in Figure 4.5(a-b) respectively. Bend contours are observed in the bright field image, which could be attributed to the thinness of the sample. The diffraction pattern in Figure 4.5(b) can be indexed to [100] zone axis of NiMnSb. Clear four-fold symmetry can be observed in the pattern. The partially circular rings have formed due to the formation of very fine particles while ultrasonication of the NiMnSb alloy, which can be seen in the bright filed image. The calculated lattice parameter also matches with the NiMnSb alloy as observed in the XRD pattern. Even though semi-Heusler NiMnSb alloy is an ordered structure, contrary to the general perception,

superlattice reflections are not observed in the diffraction pattern in Figure 4.5(b). It is worth pointing out that the underlying lattice of semi-Heusler NiMnSb is FCC and its void positions are filled in an ordered manner. Superlattice reflections are observed when ordering takes place in the FCC positions of the lattice changing the FCC lattice to primitive lattice type. TEM bright field image of the semi-Heusler NiMnSb alloy along [111] zone axis and its rotationally oriented diffraction pattern are given in Figure 4.5(c-d). In the diffraction pattern in Figure 4.5(d), three-fold rotational axis of symmetry is observed, indicating the lattice to be cubic. The d-spacings and the lattice parameter as calculated from the diffraction pattern matches quite closely with the semi-Heusler NiMnSb alloy. In the bright field image in Figure 4.5c, dislocations are observed. Appearance of the dislocation indicates that it is most likely a mixed type dislocation. It is further confirmed that the dislocation lies along [110].

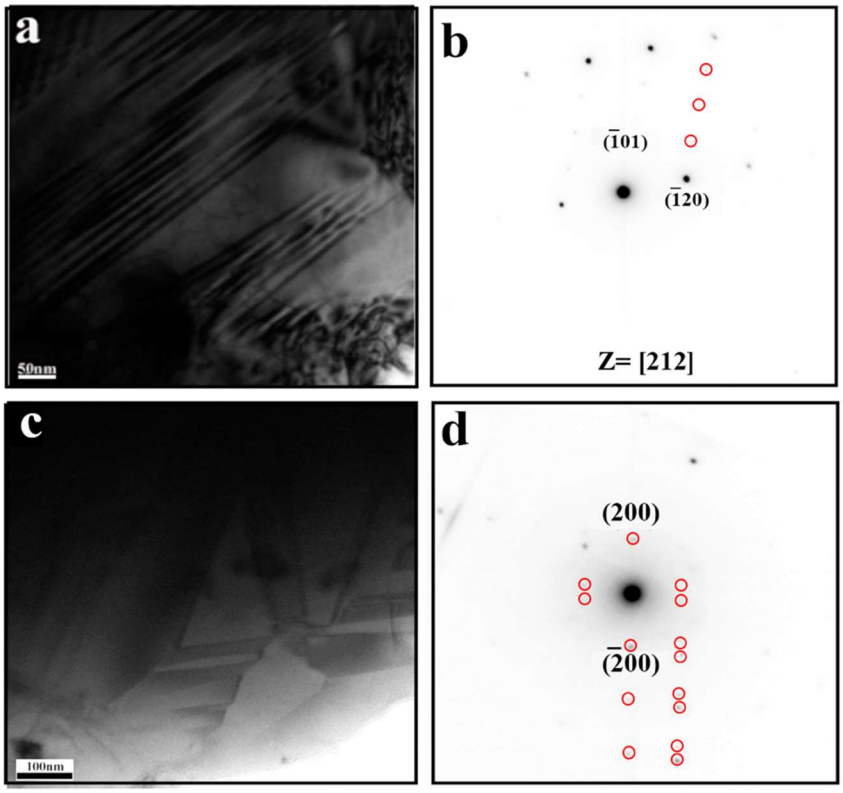

Figure 4.6: (a, c) TEM bright field images and (b,d) corresponding rotationally oriented electron diffraction patterns from the SbV_3 phase in the induction melted and as-solidified NiMnSbV alloy. In the bright field image in (a), linear contrast is observed due to the layered structure of the compound and due to the presence of defects in the phase. The corresponding electron diffraction pattern in (b) along Z= [212] shows that

the phase is cubic and the presence of the superlattice reflections (marked with red arrows) confirms that the phase repeats in every fourth layer. In the bright field image in Figure 4.6(c), linear contrast typical of twins can be observed and it is confirmed through the electron diffraction pattern in (d), in which 200 is the unique row of reflections signifying that the twin planes are {200} type.

TEM bright field image and its corresponding diffraction pattern from the SbV_3 phase in the as-solidified NiMnSbV are given in Figure 4.6(a-b). In the bright field image in Figure 4.6 (a), from the body of the SbV_3 phase, finely spaced linear contrast typical of planar faults could be observed. The corresponding diffraction pattern in Figure 4.6(b) matches with [212] zone axis pattern of SbV_3 phase. The lattice parameter and the d-spacings match quite closely with the XRD pattern of the SbV_3 phase. More importantly, three superlattice reflections along 101 type reciprocal lattice vector could be observed. The origin of this superlattice reflection would be discussed in conjunction with the structure in the discussion section. Higher magnification bright field image of the twinned region in SbV_3 phase and its corresponding diffraction pattern are given in Figure 4.6(c-d). In the diffraction pattern, it is observed that 200 is the unsplitted row of reflections. Other spots in the diffraction pattern are related to one another by 180º rotation around the perpendicular to the 200 vector. It can be concluded from this diffraction pattern that the planar faults are compound twins in which 200 is the twin plane or the composition plane.

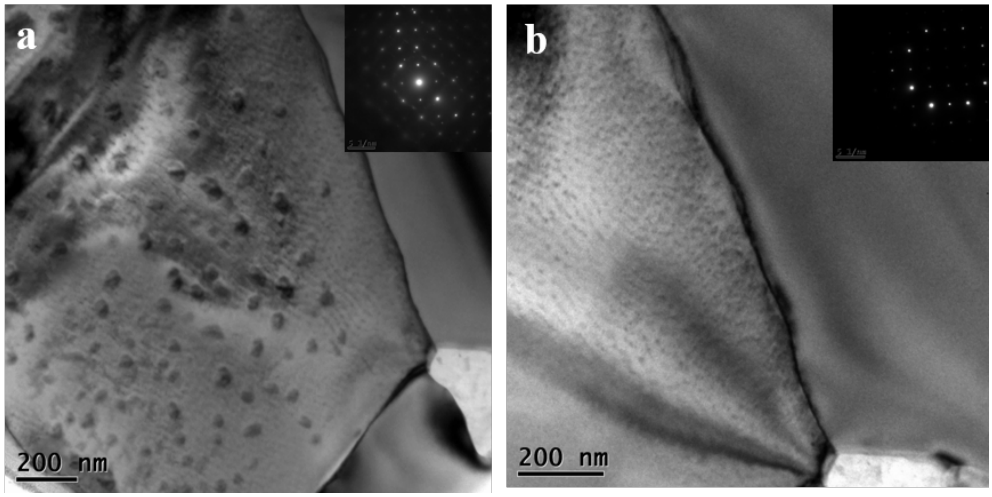

Figure 4.7: (a) in-situ TEM bright field image of NiMnSbV as-solidified alloy captured at 400˚C, where the nucleation of (Ni/Mn)Sb phase can clearly be seen in

NiMnSb phase which is oriented along [100] and (b) the interface of NiMnSb and SbV_3 , where SbV_3 does not show any phase transformation.

The in-situ heating stage TEM was also carried out for the confirmation of the observation made by in-situ heating stage X-ray diffraction. The investigation was carried out at 400˚C. Figure 4.7(a) shows the nucleation of (Ni/Mn)Sb phase alongwith the matrix of NiMnSb which is aligned at [100] zone axis. The diffraction patterns are placed as insets in their corresponding bright field images. Figure 4.7(b) represents the interface of NiMnSb and SbV_3 which does not show any orientation relationship, however, it can clearly be seen in the bright field image that NiMnSb shows phase transformation but SbV_3 does not show any kind of phase transformation which confirms the observation made by the X-ray diffraction.

4.4 Discussion

Systematic investigation on NiMnSb and NiMnSbV alloys through x-ray diffraction and microscopy brings out important information in relation to phase formation, stability, microstructural evolution and defects in these alloys. Additionally, it shades light on the empiricism that exists around the design strategy for high entropy alloys (HEAs)/complex concentrated alloys (CCAs)/ multi-principal elemental alloys (MPEAs). It has been discussed in the following sections.

4.4.1 Phase formation and stability

In NiMnSb and NiMnSbV alloys, Ni, Mn and V are transition metals and Sb is a metalloid located in the p-block of the periodic table. The atomic radii of Ni, Mn, Sb and V are 1.97 Å, 2.05 Å, 2.06 Å and 2.07 Å respectively. NiMnSb has been reported to form semi-Heusler phase. However, its temperature dependent stability has not been determined with certainty. In NiMnSb alloys surface segregation of Mn and Sb has been observed earlier [131]. However, it is not clear whether the segregation was due the instability of the phase at higher temperatures or due to the processing condition that was adopted while processing the alloy. In the present study, it has been clearly observed that the semi-Heusler NiMnSb phase is not stable beyond 400^{o}C and it nucleates hexagonal (Ni/Mn)Sb intermetallic phase. The (Ni/Mn)Sb phase grows at the expense of the original semi-Heusler NiMnSb phase. Similarly, the semi-Heusler phase in the

NiMnSbV alloy, which is partly doped with V is also not stable beyond 400^{o}C and it nucleates the same phase, which grows at the expense of the original semi-Heusler phase that is present in the alloy. Lack of stability at high temperature for the semi-Heusler NiMnSb alloy may be a major impediment for this alloy so far, its application as thermoelectric material is concerned. However, the SbV_3 phase in the NiMnSbV alloy is found to be stable in the temperature range of investigation in the present study.

It has been widely reported in HEAs/CCAs/MPEAs literature that systematic substitution in the crystal lattice is one of the viable routes to design these alloys. However, only a very limited number of alloys have been discovered so far that forms single phase solid solution (SPSS) or single phase intermetallic [129,132]. Additionally, their temperature dependent stability is also not determined unambiguously. The present study was taken up to revisit the hypothesis that systematic substitution in the crystal lattice may be a viable route to design single phase multicomponent intermetallic alloys. The atomic size mismatch values between Ni, Mn, Sb and V are given in Table 4.1. It is observed from the Table 4.1 that the atomic size mismatch between Ni-Mn, Ni-Sb and Mn-Sb are ~ 4%, 4.5% and 0.4% respectively. All the binary atomic size mismatch values are less than 12%, which is an essential criterion for solid solution formation according to Hume-Rothery rule. The binary enthalpy of mixing values for all the above elements are given in Table 4.2. The binary enthalpy of mixing values indicates that it is highly negative for Ni-Mn and Mn-Sb. However, the same is only mildly negative for the Ni-Sb combination. However, a good number of intermetallic phases are observed in all the binaries i. e. Ni-Mn, Ni-Sb and Mn-Sb phase diagrams. This observation further reinforces the idea that phase formation problem in the light of binary atomic size mismatch or enthalpy of mixing is only empirical. Total energy minimization is the defining criteria so far, the phase selection is concerned. In a similar line, it is observed that when Ni, Mn and Sb are alloyed in equi-atomic proportion, it forms semi-Heusler intermetallic phase.

Table 4.1:Relative difference in atomic radii (in %) between Ni, Mn, Sb and V

	Ni	Mn	Sb	V
Ni	0	4	4.5	5
Mn	4	0	0.4	0.97
Sb	4.5	0.4	0	0.48
V	5	0.97	0.48	0

Table 4.2:Binary Enthalpy of mixing at infinite dilution between Ni, Mn, Sb and V (kJ/mol)

	Ni	Mn	Sb	V
Ni	0	-33	-4	-69
Mn	-33	0	-35	-3
Sb	-7	-61	0	-40
V	-75	-3	-25	0

In order to form NiMnSb semi-Heusler phase based multicomponent alloy, V was chosen as a suitable substituting element. It is observed from the Table 4.1 that atomic size mismatch between V and Ni, Mn, Sb are ~5%, 1% and 0.5% respectively. Ideally, vanadium should be able to substitute any of the atomic sites without introducing a large amount of strain in the lattice. Additionally, the enthalpy of mixing values of V with Ni and Sb are highly negative, which should stabilize the semi-Heusler NiMnSb phase. However, contrary to the expectation, upon vanadium addition the alloy forms two

phase microstructure consisting of semi-Heusler NiMnSb and cubic SbV_3 phases. This proves further that systematic substitution based on atomic size mismatch and binary enthalpy of mixing, in the lattice of an intermetallic phase is not always the viable route to design multicomponent single-phase intermetallic alloys.

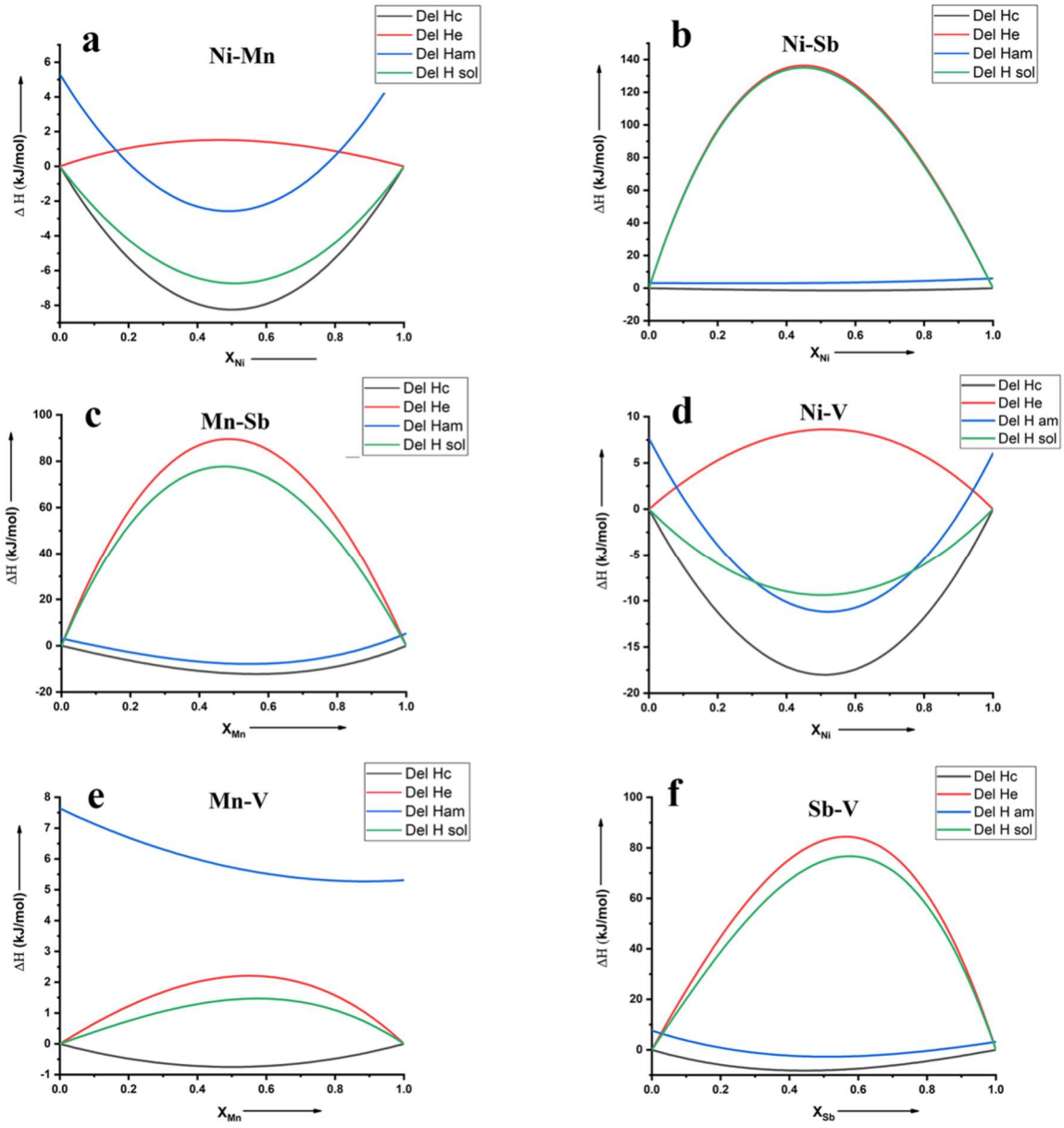

Figure 4.8: Change in enthalpy (ΔH) vs. composition plots for binaries (a) Ni-Mn (b) Ni-Sb (c) Mn-Sb (d) Ni-V (e) Mn-V (f) Sb-V as calculated by Miedema's model. ΔH solid solution (Del H sol), ΔH amorphous (ΔH am), ΔH elastic (ΔHe) and ΔH chemical (ΔHc) are plotted in green, blue, red and black respectively for all the binary systems.

Phase formation and stability of binary, ternary and higher order alloys have been studied through Miedema's model [133] mostly for transition metal containing alloy systems. Though the model has been extended to ternary alloy systems [134,135], it must be spelt out that due to the lack of thermodynamic data, ternary interaction coefficients were neglected. Moreover, electronic enthalpy component was also neglected assuming it to be very small. In the present work also, attempt has been made to understand the phase formation and stability in NiMnSb and NiMnSbV alloys through Miedema's model. Binary enthalpy of solid solution formation (ΔH_{sol}), enthalpy of amorphous phase formation (ΔH_{am}), chemical enthalpy of mixing (ΔH_c) and elastic enthalpy of mixing (ΔH_e) for binaries Ni-Mn, Ni-Sb, Mn-Sb, Ni-V, Mn-V and Sb-V are given in Figure 4.8(a-f). It is observed from the calculations that the enthalpy of solid solution formation for Ni-Mn is always more negative than the enthalpy of amorphous phase formation for the same alloy system. It is quite understandable as the atomic size mismatch between Ni and Mn is ~4% and the chemical enthalpy of mixing of Ni and Mn at infinite dilution is highly negative. However, the picture is quite different for Ni-Sb and Mn-Sb. For Ni-Sb and Mn-Sb the enthalpy of amorphous phase formation is more negative than the enthalpy of solid solution formation. It might be possible to form the amorphous phase in this system under non-equilibrium processing conditions. The atomic size mismatch of Ni and Mn with Sb is only ~4.5% and 0.5% respectively. The chemical enthalpy of mixing at infinite dilution for Ni and Mn with Sb is mildly negative and highly negative respectively. They also should form binary solid solution and intermetallic phases. In the phase diagrams of Ni-Mn, Ni-Sb and Mn-Sb a good number of intermetallic phases along with solid solution phases could be observed. A closer look at the chemical enthalpy (ΔH_c) and elastic enthalpy (ΔH_e) indicates that for Mn-Sb and Ni-Sb the elastic enthalpy component is very high at equi-atomic composition which might be attributed to the bulk modulus of Sb. It is expected that when Ni, Mn and Sb are mixed together in equi-atomic proportion, presence of Sb should make the elastic enthalpy component very high, which in turn might destabilize the lattice. However, NiMnSb semi-Heusler intermetallic phase is formed in the alloy. It must be inferred from this observation that ternary self-interaction coefficient must play an important role, which has been neglected so far. Additionally, the electronic component of enthalpy also should not be neglected in order to predict and substantiate the phase formation more accurately.

The interaction of V with Ni, Mn and Sb has also been studied through Miedema's model (Figure 4.8(d-f)). In the Ni-V system, the enthalpy of formation of amorphous phase is more negative than the enthalpy of formation of solid solution phase over a composition range of ~30-75 at%. In this composition range it might be possible to form the amorphous phase by non-equilibrium processing techniques. In the Ni-V phase diagram within the same composition range intermetallic phases are observed. However, for Mn-V and Sb-V systems, the solid solution phase is more stable than the amorphous phase over the entire composition range. The elastic enthalpy of mixing increases steeply upon addition of V with Ni, Mn and Sb. However, the rate of increase is quite high with Sb. It has been observed that addition of Sb with Ni and Mn also increases the elastic enthalpy of mixing. Probably due to the electronic factor and due to the ternary self-interaction parameter, NiMnSb semi-Heusler intermetallic phase gets stabilized when they are mixed in equi-atomic proportion. Addition of V further increases the elastic strain and it has got a destabilizing effect on the semi-Heusler NiMnSb intermetallic. That is why, in the NiMnSbV alloy apart from semi-Heusler NiMnSb phase, additional SbV_3 phase is also observed. The atomic radii mismatch between Sb and V is very small (~0.48%) and their enthalpy of mixing being highly negative, they form the intermetallic SbV_3 phase. It appears from the present study that systematic substitution with minimal atomic radii mismatch cannot be the sole criteria for designing single phase HEAs. Binary, ternary, quaternary thermodynamic self-interaction parameters as well as the electronic contribution should be taken into account. As a whole the problem is extremely complicated and a comprehensive model-based approach is required to develop a robust alloy design strategy.

4.4.2 Microstructural evolution

The as-solidified NiMnSb alloy forms semi-Heusler phase as has been confirmed by the XRD and electron diffraction. In this alloy, solidification shrinkage porosities are observed. However, in the NiMnSbV alloy, blocky SbV_3 phase is dispersed in the matrix of semi-Heusler NiMnSb phase. The blocky SbV_3 phase is mildly faceted. The composition analysis of the semi-Heusler NiMnSb and SbV_3 phases indicates that minor amount of V is dissolved in the semi-Heusler phase and minor quantities of Ni and Mn are dissolved in the SbV_3 phase. This clearly indicates that a composition segregation takes place when the alloy solidifies. This is further substantiated by the presence of

dendrites/lamellae at the interfaces of semi-Hesuler NiMnSb and SbV_3. Even though the sequence of nucleation of NiMnSb and SbV_3 phase cannot be determined, it is inferred from the observation that while solidification, NiMnSb/(Ni/Mn)Sb nucleates independently and while solidification it partially rejects V. As a result, the surrounding region with NiMnSb/(Ni/Mn)Sb becomes enriched with Sb and V where SbV_3 phase may nucleate. In case the SbV_3 phase nucleates first, the surrounding region would be enriched in Ni and Mn, which would facilitate the nucleation of the NiMnSb/ (Ni/Mn)Sb phase. The size and the separation of the dendrites is strongly correlated with the local heat transfer conditions during solidification. The faceted nature of SbV_3 is also indicative of the tendency of the SbV_3 phase to minimize its interface energy with the semi-Heusler NiMnSb phase. The melting point of SbV_3 is ~ 1230^{o}C. It is quite likely that SbV_3 phase nucleates first while the alloy is solidified, leaving the remaining liquid alloy rich in Ni, Mn and Sb. Additionally, it has been observed through in-situ XRD that semi-Heusler NiMnSb phase is not stable beyond 400^{o}C and it transforms to hexagonal (Ni/Mn)Sb phase. The melting points of hexagonal NiSb and MnSb are 1147^{o}C and 840^{o}C respectively. It is also possible that hexagonal (Ni/Mn)Sb nucleates first leaving the remaining liquid rich in V, which facilitates the nucleation of SbV_3 phase. At a later stage, while cooling, hexagonal (Ni/Mn)Sb transforms into semi-Heusler NiMnSb phase. Entire phase transformation sequence leading to the development of this microstructure will require detailed in-situ microscopic observation.

4.4.3 Structure and defects in NiMnSb and NiMnSbV

Heusler alloys can be structurally classified into several groups i.e. Full Heusler (A_2BC), Inverse Heusler (A_2BC), semi-Heusler (ABC) and Quaternary Heusler (AA'BC) [15]. In Full Heusler alloy A_2BC, the A atoms occupy the FCC position and the octahedral void positions, the B and C atoms occupy the alternate tetrahedral void positions. In Inverse Heusler A_2BC, half of the A atoms occupy the FCC positions and the remaining half occupy half of the tetrahedral void positions alternately, the B atoms occupy the octahedral void positions and the C atoms occupy the remaining half of the alternate tetrahedral void positions. In semi-Heusler ABC alloy, the A atoms occupy the FCC positions, the B and C atoms occupy the alternate tetrahedral void positions. In Quaternary Heusler AA'BC, the A atoms occupy the FCC positions, the A' atoms occupy the octahedral void positions, the B and C atoms occupy the alternate tetrahedral voids

positions. In all the structures, the underlying lattice remains to be FCC. In the present study, semi-Heusler phase is observed in NiMnSb and in NiMnSbV alloys. However, the semi-Heusler phase in both the alloys is not stable beyond 400ºC and hexagonal (Ni/Mn)Sb phase forms at the expense of the semi-Heusler phase. The structure of hexagonal (Ni/Mn)Sb is hP4 and it has ….ABAC… kind of stacking along [0001]. There is no polymorphic relationship that can be established between the semi-Heusler and the hexagonal (Ni/Mn)Sb phase. It is concluded from this observation that (Ni/Mn)Sb phase nucleates and grows at the expense of the parent semi-Heusler phase, which is purely driven by thermodynamics.

In the NiMnSbV alloy, apart from the semi-Heusler phase, SbV_3 phase is also observed. The strukturbericht notation of this phase is A15. The structure of SbV_3 was initially assumed to be a prototype of β-W [136]. The Pearson symbol, space group and the lattice parameter of this phase is cP8, $Pm\bar{3}n$ and ~4.94Å respectively. A polyhedral diagram showing the coordinated environments of antimony and vanadium atoms are shown in Figure 4.8(a-b) respectively.

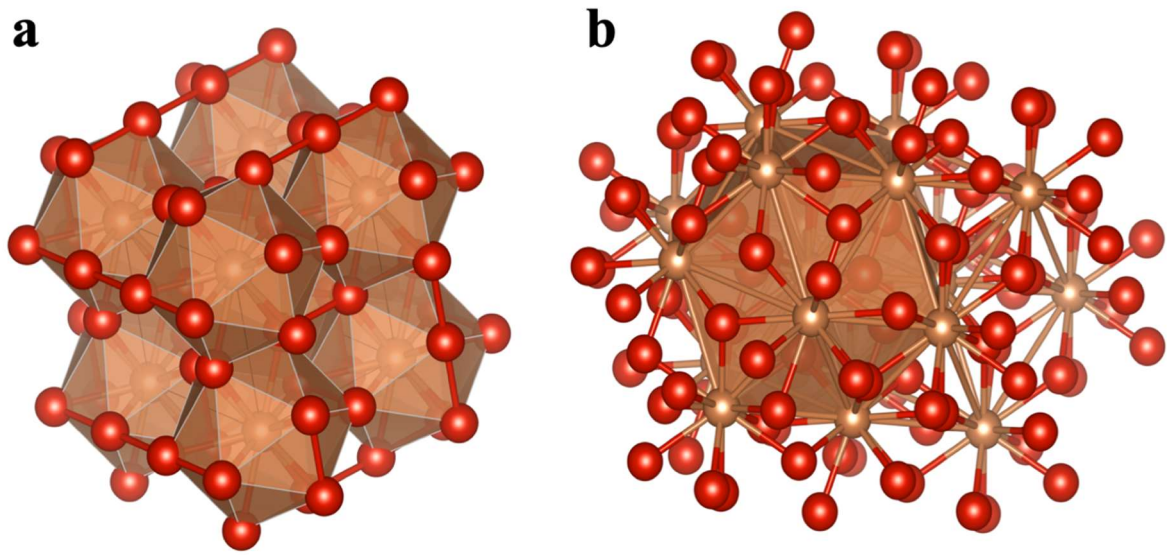

Figure 4.9: Polyhedral diagram for cubic SbV_3 phase. (a) Edge sharing 12-fold coordination icosahedra with Sb atom at the center (b) 14-fold coordination polyhedra with V atom at the center.

It is observed that (Figure 4.9a) all the corner positions and the body centered position of the basic cubic lattice are occupied by Sb. However, the resulting structure turns out to be primitive cubic. This is attributed to the coordination environment of the Sb atoms located at the corners and at the body centering position. The body centered Sb is 12-fold coordinated and the corner Sb atoms are 14-fold coordinated. So, the Sb atoms at the body centering position and at the corner positions are no equivalent, resulting into a primitive symmetry of the cubic lattice. This is why superlattice reflections are observed in the electron diffraction pattern from SbV_3 phase (Figure 4.6b). However, the coordination environment is a subset of Frank-Kasper coordination environment [8]. SbV_3 phase can be considered as a Frank-Kasper phase. The structure can be alternatively described as an edge sharing network of icosahedra with the Sb atom at the center and the V atoms at the vertices of the icosahedra. However, the 12-fold coordinated icosahedral cluster is likely to be distorted due to the atomic size difference between Sb and V, which is 0.5% (Table 4.1). It has been pointed out earlier that for ideal topological packing of icosahedral clusters, ~12% atomic size difference is the ideal value [137,138]. However, Cr_3Si prototype A15 structures form at the radius ratio value close to unity. It can be concluded from this observation that the icosahedral clusters in A15 structures are distorted in nature. While solidification of NiMnSbV alloys, solute segregation takes place, and in theV rich regions such distorted clusters form that ultimately results in the nucleation of the SbV_3 phase.

As SbV_3 phase is a topologically close packed Frank-Kasper compound, it has distorted clusters (Figure 4.8(a-b)). Defects could be inherent to this structure. Solid solutioning and solid-state phase transformation induced strain (Hexagonal (Ni/Mn)Sb → Cubic NiMnSb) is likely to increase its defect density. XEDS studies indicates that minor amount of Ni and Mn is dissolved in the SbV_3 phase in the NiMnSbV alloy, which is probably the reason as to why extended defect density are seen in the phase. The twinning reported in Figure 4.6(c-d) indicates that it is a compound deformation twin. Such twins have been reported in this phase earlier [139].

4.5 Conclusions:

Following conclusions can be drawn from the present study

1. In the as solidified NiMnSb alloy, cubic semi-Heusler NiMnSb phase and in the NiMnSbV alloy, cubic SbV_3 phase along with the semi-Heusler NiMnSb phase are observed.
2. The SbV_3 phase nucleates and grows in the NiMnSbV alloy through solute rejection process. It is mildly faceted and lamellar structure is observed at the interface of SbV_3 with semi-Heusler NiMnSb phase.
3. The SbV_3 phase is stable up to 700^{o}C, while the semi-Heusler NiMnSb phase is not stable beyond 400 ^{o}C and it transforms into hexagonal (Ni/Mn)Sb phase.
4. The Cubic SbV_3 is a Frank-Kasper phase. In this phase, edge sharing 12-fold coordinated icosahedral clusters and 14-fold coordinated clusters are observed. The clusters are distorted, which might be a possible reason behind extensive formation of compound twins in this structure.
5. Systematic substitution in the lattice of semi-Heusler NiMnSb alloy based on binary enthalpy of mixing and atomic radius mismatch may not be the ideal design strategy for the development of semi-Heusler NiMnSb based single phase multicomponent/high entropy alloys.